

# Photocatalytic evaluation of supported ilmenite on clay substrates for degradation of organic dyes

N. Ramos-Domínguez, D. Vallejo-Rendón, F. Caballero-Briones

Titanium dioxide (TiO<sub>2</sub>) is widely used as a photocatalyst for the degradation of organic pollutants in water. However, to improve its absorption in the visible range and enhance the potential of photocatalysis for water treatment, the incorporation of Fe into TiO<sub>2</sub> or the use of its natural mineral form, such as ilmenite (Fe<sup>2+</sup>Ti<sup>4+</sup>O<sub>3</sub>), has been widely studied. However, the effects of the different compositions in natural ilmenite minerals on the photocatalytic degradation of dyes has not been revised. In this study, the photodegradation of methylene blue (MB) and methyl orange (MO) dyes was studied using five different ilmenite minerals under UV and visible light irradiation. For the case of visible light photocatalysis a pilot scale reactor was tested. The ilmenites were characterized by diffraction (XRD), X-ray fluorescence (XRF) and diffuse reflectance spectroscopy (DRS). Crystalline phases included rutile, pseudorutile, and ilmenite. The Fe/Ti ratio in the ilmenites was between 1:10 to 1:1, while V and Mn were found as minor impurities (0 to 2 wt% Mn, and 1.0 to 1.6 wt% V). Band gap energies vary with the Fe/Ti ratio from 2.18 to 2.83 eV. Photodegradation experiments were conducted with an initial dye concentration of 6 mg/L, over three cycles of 200 minutes, collecting samples at various time intervals. Under UV light, degradation percentages for MB and MO ranged from 48 to 90% and 26 to 74%, respectively, by the end of the third degradation cycle. Under visible light, samples with the higher Ti/Fe ratio (M3 and M5) achieved 61.10% and 57.73% degradation of MB, respectively. No degradation was observed for MO under visible light, while MB degradation was attributed to a sensitization effect on TiO<sub>2</sub>. The differences in photocatalytic efficiency between dyes were attributed to their molecular structures, to the Fe/Ti ratios and the V and Mn impurities in the ilmenites, although further work is required to differentiate between these effects. The work demonstrated the feasibility of using natural ilmenites for dye photodegradation, as well as to set a pilot scale reactor for visible light treatments.



## Introduction


Water contamination by organic compounds can be alleviated through physical, chemical, and electrochemical methods. Among the chemical methods, photocatalysis, an advanced oxidation process (AOP) that consists of the degradation of contaminants through light induced oxidation-reduction reactions, has advantages such as no sludge production, few harmful by-products, and instantaneous removal of organic pollutants [1]. Among commercial organic dyes, azo dyes are the more abundant type, accounting for 65 to 75% of all textile products. In addition, there are also dyes that contain a nitro group in their structure, which are mutagenic, highly toxic, and can generate dangerous by-products after the molecule breaks down [2]. Thus, there is a need to implement treatments for degradation of these compounds, including studies about mechanisms, strategies, photocatalytic reactor designs, operating conditions, among others [3].

TiO<sub>2</sub> and ZnO are photocatalytic materials used for the degradation of pollutants due to their stability, availability, and photocatalytic activity [4-8]. However, they have limitations due to their wide bandgap which limits their activity to the ultraviolet light. In this regard, TiO<sub>2</sub> doped with different Fe contents (1–3 %wt) lead to a reduction in the bandgap from 3.2 eV to 2.1 eV and higher degradation efficiencies of reactive red 198, compared to undoped TiO<sub>2</sub> [9]. In another study, Fe-TiO<sub>2</sub> nanoparticles with nominal Fe contents from 0.35 to 7.0 wt% were prepared; the band gap reduced from 3.17 to 2.58 eV with the Fe contents. The better phenol photodegradation was achieved with a sample with a nominal Fe content of 0.7 wt% and H<sub>2</sub>O<sub>2</sub> as oxidant [10].

On the other hand, ilmenites are materials with general composition Fe<sub>x</sub>Ti<sub>y</sub>O<sub>z</sub> which are a promising alternative due to their low cost and natural abundance, while having absorption capacity in the visible light range [11]. In this

regard, the properties and photodegradation kinetics of Reactive Black 5 dye (RB-5) were studied onto a natural ilmenite from Malaysia, with a band gap of 2.5 eV; the ilmenite displayed both rutile (TiO<sub>2</sub>) and ilmenite (FeTiO<sub>3</sub>) diffraction peaks. A maximum photodegradation efficiency of RB-5 of 73 %, with first order kinetics was achieved under simulated solar irradiation [11]. Another study used an unrefined natural ilmenite, with FeTiO<sub>3</sub>, hematite (Fe<sub>2</sub>O<sub>3</sub>) and rutile as main phases, to photodegrade two perfluoroalkyl compounds in the presence of UV-C light, with a maximum photodegradation of 80 % in three consecutive degradation cycles [12]. From a natural ilmenite ore from Indonesia, a photocatalyst with an enriched TiO<sub>2</sub> with Mn and Cr impurities was prepared by a combination of a roasting process and acid leaching to decompose Eriochrome Black-T with low power UV light; a maximum degradation of 83% was achieved [13]. Another report showed the use of a natural ilmenite previously processed in a ball mill and leached in H<sub>2</sub>SO<sub>4</sub>, for the photo Fenton degradation of methylene blue (MB) and methyl orange (MO),

Naian Ramos-Domínguez , Felipe Caballero-Briones   
*Instituto Politécnico Nacional, Materiales y Tecnologías para  
 Energía, Salud y Medio Ambiente (GESMAT), CICATA,  
 Altamira, TAM, 89600, México.*

Dulce Vallejo-Rendón   
*Universidad Tecnológica de Altamira,  
 Altamira, TAM, 89608, México.*

Presented at the Renewable Energy: Materials and Devices Symposium,  
 XVIII Intl. Conf. Surfaces, Materials, and Vacuum, SMCTSM,  
 September 22<sup>nd</sup> to 26<sup>th</sup>, 2025. Puebla, PUE, Mexico.

Received: September 23rd, 2025.

Accepted: March 5th, 2026.

Published: April 23rd, 2026.

© 2026 by the authors. Creative Commons Attribution  
[https://doi.org/10.47566/2026\\_svv39\\_1-260401](https://doi.org/10.47566/2026_svv39_1-260401)

in the presence of  $\text{H}_2\text{O}_2$  as oxidizing agent, using a 40 W white LED lamp as visible light source [14]. The milled ilmenite has a band gap of 3 eV and the main phases reported were  $\text{FeTiO}_3$ ,  $\text{Fe}_2\text{O}_3$  with a Fe/Ti ratio ca. 1:1, as well as  $\text{SiO}_2$ ,  $\text{Al}_2\text{O}_3$  and minor  $\text{Cr}_2\text{O}_3$  and  $\text{V}_2\text{O}_5$  impurities; the article discussed the positive role of the impurities to enhance the photodegradation activity [14]. However, despite the reports where natural ilmenites have been used for dye photodegradation, the use of supported ilmenites has not been reported so far. Two recent reviews discuss the characteristics and the selection of solid supports for photocatalyst immobilization [15,16]. Requirements of the support such as wide area to compensate the activity reduction upon immobilization, high dielectric constant to avoid charge dispersion, mechanical and chemical stability, affinity to the photocatalyst and the adhesive used to keep particles together, and easiness of the support to be removed from the solution, among other characteristics were described [15]. Among the supports studied in the literature, natural silicate minerals including porous, 1D, 2D, and 3D minerals; natural carbonate, or carbon-based mineral supports, natural sulfate or sulfide minerals, as well as the use of bulk, natural minerals such as ilmenite ( $\text{FeTiO}_3$ ) and monazite ( $\text{CeO}_2/\text{TiO}_2$ ) have been reported [16].

In this work, five natural ilmenites with different compositions were immobilized onto cooked red clay tiles (*barro cocido*) and tested for MO and MB photodegradation. Cooked red clay was chosen as solid support because of its wide availability, chemical, thermal, and mechanical stability. The photodegradation efficiency in UV-C and visible light was compared and discussed in terms of the Fe/Ti ratio, the band gap, and the presence of potentially active impurities in the samples.

## Experimental

### Natural ilmenites and photocatalyst immobilization

Samples of four different ilmenites from undisclosed batches, labelled as M1-M4, were received as a donation of a local supplier; the M5 sample was acquired from Solargil, France (Ilmenite,  $\text{FeTiO}_3$ ). The granular natural ilmenites (300 mesh) were used without prior treatment. The photocatalytic formulation was prepared with a 10:1 wt./vol. proportion of the ilmenite particles and antibacterial, white vinyl paint (Comex, Mexico) as adhesive, dispersing the ilmenite by thorough mechanical agitation using a vortex mixer. The resulting mixture was applied onto cooked red clay tiles using a paintbrush until the pores were filled and the clay surface was completely covered (three paint hands) and left to dry for at least twelve hours, as depicted in Figure 1. For the photocatalysis studies, the clay tile sections not exposed to the light source were coated with transparent nail varnish to avoid absorption of the dye solution.

### Characterization

The crystal structure of the ilmenites was analyzed by X-ray diffraction (XRD) in a D-8 Advance diffractometer (Bruker, Germany) at 40 kV and 30 mA, using a  $\text{Cu K}\alpha$  radiation tube ( $\lambda = 1.54 \text{ \AA}$ ), over a  $2\theta$  range from 20 to  $70^\circ$  with a step size



**Figure 1.** Formulation (1), particle dispersion (2) and coating (3) of the photocatalyst onto the red cooked clay tiles.

of  $0.02^\circ$ . The elemental composition of the ilmenites was determined by X-ray fluorescence (XRF) using a Mesa 50 spectrometer (Horiba, Japan) operating at 50 kV. Powders were put into a cell over an X-ray transparent membrane, X-ray were focused through a 3 mm collimator, with measuring time of 100 seconds. Quantification was made with instrument software without standards. Diffuse reflectance spectroscopy (DRS) was performed in an Agilent Technologies Cary 5000 series spectrophotometer (Santa Clara, CA, USA) in absorbance mode, with the analysis carried out over a wavelength range of 200-850 nm. To determine the forbidden band gap of the ilmenites, the Kubelka-Munk and Tauc formalisms were used [17].

### Photocatalytic degradation experiments

The laboratory-scale, UV photodegradation experiments were carried out in a batch reactor consisting of a glass cylinder containing 0.4 L of a 6 mg/L solution of each dye, *i.e.* methyl orange (MO, 99% purity Fagalab, Mexico) and methylene blue (MB, 99% purity, Fagalab, Mexico), stirred with a magnet bar. Two tiles of cooked red clay with dimensions 1 x 2 x 12 cm, coated with the photocatalyst formulation as described above, were introduced in the solution facing the illumination source, which was a 7 W UV-C lamp (200-284 nm, peak @254 nm). The photolysis blank was performed illuminating the system with the tiles only coated with the paint. The adsorption blank was done by exposing the coated tiles to the MO and MB solutions without illumination. The reactor was placed inside a dark box, and three degradation cycles of 200 min each one were performed. 1 mL aliquots were taken at 2, 5, 10, 20, 50, 100,

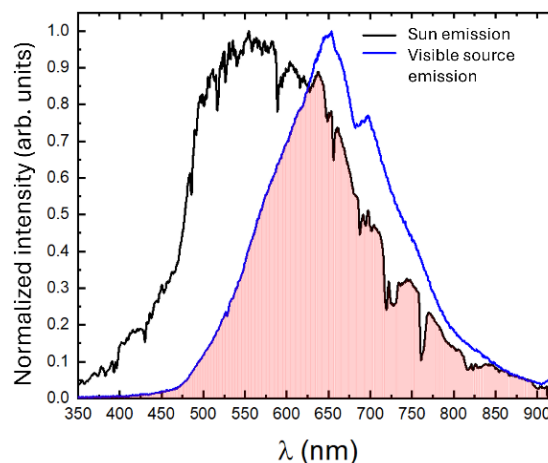


**Figure 2.** Normalized Sun irradiance vs the normalized spectrum of the tungsten-halogen lamp used in this work.

and 200 minutes to measure the absorbance with a Green Wave spectrometer and a SL1 tungsten-halogen lamp (Stellar Net, USA) in a quartz cell with 1 cm of optical path.

For the pilot scale test, a thin film reactor built with two red cooked clay tiles of 20 x 20 cm, coated with the photocatalytic formulation, was implemented. A volume of 5 L of the test solution with the same dye concentration was used. The solution recirculated over the photocatalyst supports, which were illuminated with a laboratory-set tungsten-halogen light source with maximum irradiance at 652 nm for a total irradiance of 200 W/m<sup>2</sup> measured with a pyranometer near the tile surface. The lamp spectrum is compared against the Sun irradiance in Figure 2. The same sampling, blanks and absorbance measurements were done to calculate the degradation.

The degradation activity was determined from the relation of absorbance  $A$  with the concentration  $c$ , measured by optical spectroscopy, using the Beer-Lambert's law shown in Equation 1,

$$A = \epsilon lc \quad (1)$$

where the absorbance  $A$  at 664 nm for MB, and at 464 nm for MO were used, using as extinction coefficients  $\epsilon = 25100$  @464 nm for MO [18] and  $\epsilon = 74028$  @665 nm for MB [19]. The degradation efficiency ( $D$  %) was calculated with Equation 2.

$$D\% = \frac{C_0 - C}{C_0} \times 100 \quad (2)$$

where  $C_0$  is the initial dye concentration and  $C$  the concentration after a given reaction time calculated with Equation 1 [12].

## Results

### Phase composition of the ilmenites

Figure 3 presents the X-ray diffractograms of the five ilmenite samples (M1-M5). M1 displays diffraction peaks at 2 theta 27.53°, 36.07°, 39.34°, 41.22°, 54.28°, 56.83°, and 64.23°, associated with the (110), (101), (200), (111), (211), (220), and (310) planes of rutile (TiO<sub>2</sub>, PDF 011292), respectively; correspondingly, an halo at ca. 32° and a small peak at 53°, which can be related to ilmenite (FeTiO<sub>3</sub>) were observed, as well as a non-assigned peak at ca. 48°. M2 diffractogram presents peaks at 36.07°, 41.22°, 54.28° and 56.83°, associated with the (200), (111), (211), and (220) rutile planes, as well as defined diffraction peaks at 2 theta 32.51°, 35.28° and 53.05°, which correspond to the (104), (110) and (116) planes of rhombohedral ilmenite (FeTiO<sub>3</sub>, PDF 290733); peaks observed at 38° and 62° couldn't be assigned. M3 sample presents sharp diffraction peaks at 2 theta 27.53°, 36.07°, 39.34°, 41.22°, 54.28°, 56.83°, and 69.06°, associated with the (110), (101), (200), (111), (211), (220), and (301) planes of rutile (TiO<sub>2</sub>, PDF 011292), respectively; also, hexagonal pseudorutile (Fe<sub>2</sub>(TiO<sub>3</sub>)<sub>3</sub>, PDF 130326) was confirmed with the sharp peak at 54.52° related to the (441) plane, a peak at ca. 33° from a non-assigned plane, and another peak at 53° associated with the (801) plane. The diffractogram of sample M4 displays peaks at 27.53°, 36.07°, 39.34°, 41.22°, 54.28°, 56.83°, and 69.06°,

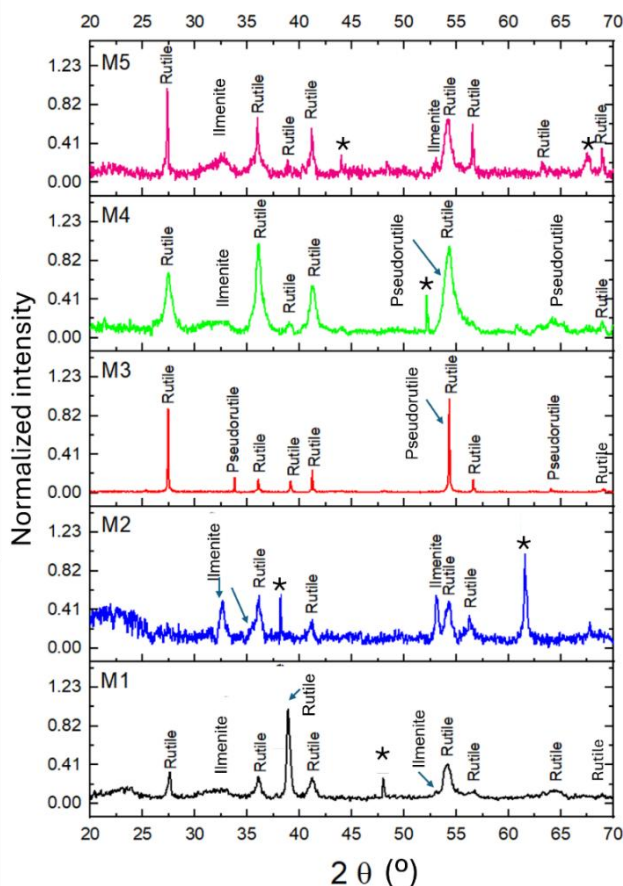
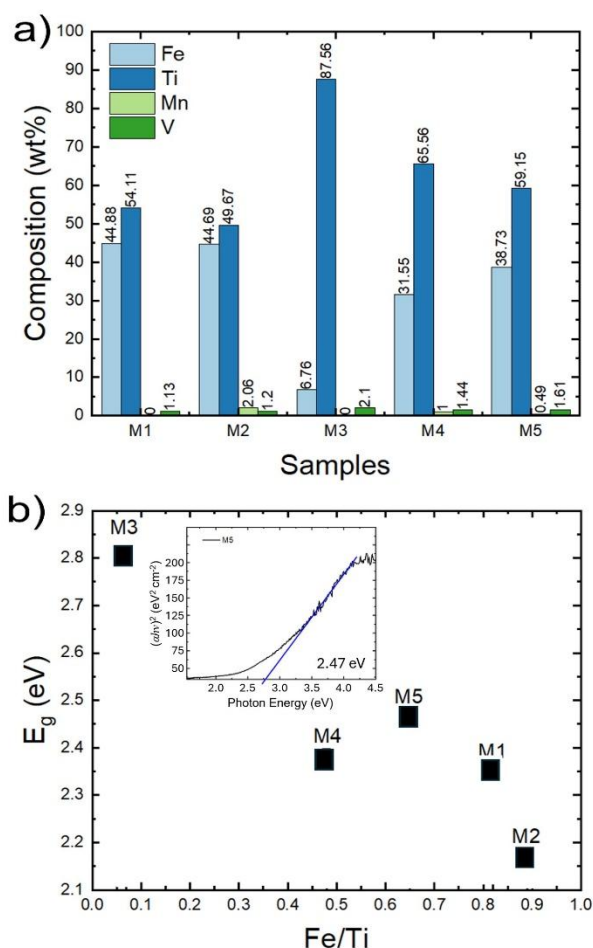


Figure 3. X-ray diffractograms of the five ilmenite samples studied in this work.

associated with the (110), (101), (200), (111), (211), (220), and (301) planes of rutile, and ilmenite-related halo at 33° and un-assigned peaks at 52° and 61°. Pseudorutile peaks were observed at 54.52° related to the (441) plane, and at 53° associated with the (801) plane. Finally, M5 shows diffraction peaks corresponding to rutile and ilmenite and an unknown peak at 44°. According to the literature, natural ilmenite minerals are mainly composed of pseudorutile rutile (TiO<sub>2</sub>), and ilmenite (FeTiO<sub>3</sub>) phases, with concentrations varying according to the ore, as suggested by the diffractograms [11-14]. Additionally, several impurities are associated with natural ilmenites such as Fe<sub>2</sub>O<sub>3</sub>, SiO<sub>2</sub>, Al<sub>2</sub>O<sub>3</sub>, MgO, CaO/CaCO<sub>3</sub>, Cr<sub>2</sub>O<sub>3</sub>, MnO/MnO<sub>2</sub>, V<sub>2</sub>O<sub>5</sub> [11-14], which may improve the photocatalytic activity by increasing oxidation in the presence of H<sub>2</sub>O<sub>2</sub> [10], by preventing charge recombination [14], enhancing light absorption [10, 20-23], or by forming active heterostructures [20-23].

### Chemical composition of the ilmenite samples

Figure 4a presents the elemental composition of the studied ilmenites. Ti and Fe are the elements accounting for more than 90 wt% of the ilmenites. The samples M1 and M2 show Fe/Ti ratios close to 1:1, while samples M4 and M5 have around 2:1 Fe/Ti respectively; correspondingly, sample M3 shows the highest difference between Fe and Ti concentration (1:10 ratio). Vanadium was found in all samples with a maximum value of 2.1 wt% in sample M3



**Figure 4.** a) Elemental composition of ilmenite samples obtained by XRF, and b) forbidden band gap with respect to the Fe/Ti ratio of ilmenite samples; inset shows the Tauc plots  $(\alpha h\nu)^2$  vs  $h\nu$  for sample M5.

and a minimum of 1.2 wt% in M1, while manganese was only detected in samples M2, M4, and M5, with a maximum concentration of 2.06 wt% in sample M2. The presence of elements such as V, Mn, Mg, and Cr is considered common in ilmenites as discussed above [11-14].

Figure 4b presents the band gap values calculated from the Tauc plots  $(\alpha h\nu)^2$  vs  $h\nu$  [17]. The  $E_g$  values in the range from 2.18 to 2.83 eV, correspond to the visible light region (438-569 nm) of the electromagnetic spectrum. The concentration of the identified elements, especially Fe, can influence the bandgap of ilmenite samples, reducing the band gap energy, as has been reported in the literature when doping  $TiO_2$  with percentages lower than 3 %wt. of Fe [10]. On the other hand, the presence of V and Mn may also influence optoelectronic behavior by forming localized states within the bandgap [20-23], which may be related with the absorption tails observed below the band gap in Figure 4b inset.

*Photocatalytic degradation with UV-light*

Immobilized photocatalysts require to be active during several cycles before been removed from the reactor to be reactivated or wasted. Therefore, cyclability of the deposited catalyst was tested by doing a first photodegradation cycle with the 6 mg/L solution either of MB or MO. After 200 min

of illumination, the light was set off for 5 minutes and a novel cycle began with the same solution; this process was done three times to assess the degradation activity after three cycles. Figure 5 presents the photodegradation percentage vs time plots of three consecutive cycles for a)  $TiO_2$  as reference material and b) M1 ilmenite; the materials were tested to degrade MB 6 mg/mL solution using UV light.

The results of total photocatalytic degradation of MB per cycle indicate that  $TiO_2$  response is stable with the number of cycles, while M1 ilmenite increases its activity in the third cycle up to 90%.

Figure 6 presents the degradation response of MB and MO for a) the ilmenites M1-M5 and  $TiO_2$ , and b) ilmenites M2 and M3, against MB in UV light in both cases, during the first degradation cycle. The respective MB and MO photolysis vs time curves in UV light are also indicated. Additionally, Figure 6a inset shows the relative improvement of photocatalytic degradation of MB in UV light of M5 vs  $TiO_2$ ; Figure 6b depicts the batch reactor scheme employed for UV photocatalytic degradation with both dyes.

It can be observed that photolysis in both dyes increases with time, possibly enhanced because the temperature increment during the cycle; future work shall consider reactor cooling to separate the temperature effects. The MB photocatalytic degradation increases above photolysis for all

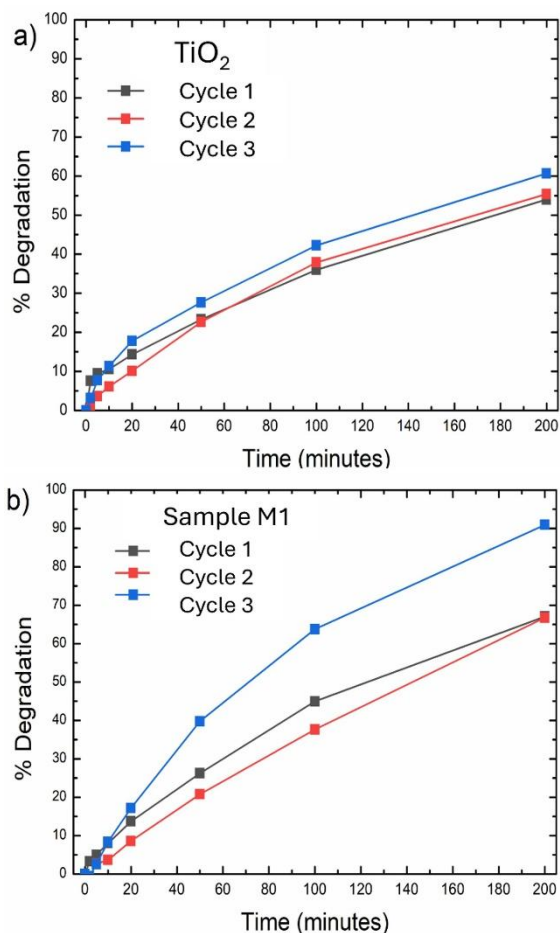


**Figure 5.** Consecutive cycles of photodegradation vs time plots of MB solution (6 mg/mL) using UV light, with supported a)  $TiO_2$ , b) M1 ilmenite.



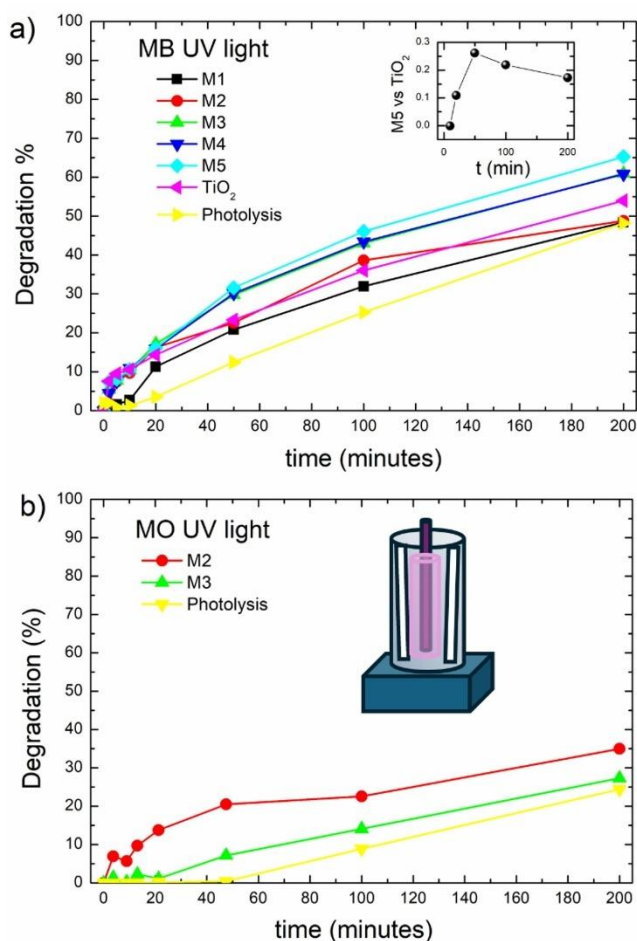


**Figure 6.** Photocatalytic degradation with UV-C light after photolysis subtraction of a) MB for the five ilmenites; inset shows the photocatalytic degradation improvement of M5 vs TiO<sub>2</sub>, b) MO for M2 and M3 samples; inset shows the photocatalytic reactor setup.

the ilmenites in the following order M1<M2<TiO<sub>2</sub><M3-M4<M5, with maximum degradation of 50% to 65% in one cycle. The improvement of degradation of M5 vs TiO<sub>2</sub> has a maximum of ca. 25%, as observed in Figure 6a inset. With respect to the MO degradation, only M2 and M3 display measurable activity above photolysis, with maximum degradation of 25-35%; for TiO<sub>2</sub> the degradation activity is below the photolysis. In contrast, Besheli *et al.* [14], reported the use of a natural ilmenite from an Iranian mine suspended in 10 mg/mL solutions of MO and MB, with and without addition of H<sub>2</sub>O<sub>2</sub> and using a white LED source. The ilmenite contained V, Cr, Si, K and Mg impurities. A complete degradation of MB and MO using a natural ilmenite was achieved; the activity improved in the presence of H<sub>2</sub>O<sub>2</sub> due to photo Fenton catalysis. The role of V and Cr impurities was not discussed [14]. The comparatively low activity reported in the present work is mostly related to the low available surface. On the other hand, reports of photodegradation using supported photocatalysts show uneven results; for example, ca. 81% removal of MB was achieved after 42 h of treatment using sunlight and a C<sub>3</sub>N<sub>4</sub> photocatalyst supported in calcium alginate spheres [24], also nano-TiO<sub>2</sub> photocatalysts supported in montmorillonite

showed a maximum degradation of 50% in one cycle, while an optimal photocatalyst load was found, which keeps high photocatalytic activity without blocking the support pores, reducing the active area [25]. Thus, to improve photocatalytic degradation, factors such as the temperature, use of a hole scavenger, the photocatalyst load into the formulation, the support porosity, and C<sub>0</sub> vs degradation capacity will be studied in future work.

*Photocatalytic degradation with visible light, pilot-scale experiments*

The pilot-scale experimental setup for visible light photodegradation was implemented as depicted in the inset of Figure 7, where the clay surface coated with the photocatalyst formulation is placed 45° with respect to the sunlight simulator; the dye solution was circulated with a 3000 L/h pump to keep a liquid film onto the tile surface. The samples M3 and M5 were tested for MB degradation. Figure 7 shows the degradation vs time of MB and the photolysis response. It can be observed that the response of M3 is above that of the photolysis, and that a maximum degradation of MB of 30% was achieved. In recent publications, supported photocatalyst in pilot-scale reactors have been reported, for example, luffa fibers were impregnated with commercial TiO<sub>2</sub> nanoparticles without any adhesion additive for the photocatalytic degradation of amoxicillin, ciprofloxacin, and tetracycline using LEDs as UV light source; with this system, the degradation rate depends on the flow rate, the number of cycles, and the geometry of the support [26]. Thus, the present study confirms the feasibility of scaling up photocatalytic degradation using supported photocatalysts. In future experiments, apart from the formulation optimization, the variation of the hydraulic residence time in the pilot scale reactor, as well as novel configurations of the support geometry will be studied.

Figure 8 presents the ln(C<sub>t</sub>/C<sub>0</sub>) vs time curves of the MB degradation in UV light (a), MB with visible light (b), and of

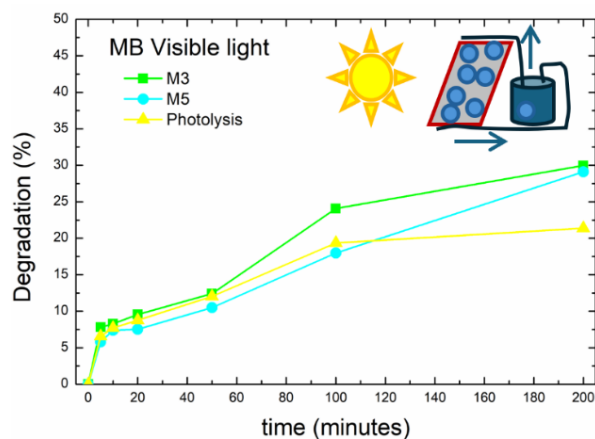


**Figure 7.** Photocatalytic degradation of MB with visible light for the samples M3 and M5. Inset: scheme of the pilot-scale reactor for photodegradation with visible light.

**Table 1.** Kinetic parameters of the photodegradation in UV and visible light of MB and MO for the different tested materials

Sample	MB						MO		
	UV light			Visible light			UV light		
	-k (min <sup>-1</sup> )	%DR <sub>max</sub>	R <sup>2</sup>	-k (min <sup>-1</sup> )	%DR <sub>max</sub>	R <sup>2</sup>	-k (min <sup>-1</sup> )	%DR <sub>max</sub>	R <sup>2</sup>
M1	0.00335	48.4	0.98028	NA	NA	NA	NA	NA	NA
M2	0.00332	48.4	0.93705	NA	NA	NA	0.00178	35.0	0.92403
M3	0.00437	60.8	0.98761	0.00145	30.0	0.99358	0.0016	27.30	0.99136
M4	0.00458	60.8	0.97807	NA	NA	NA	NA	NA	NA
M5	0.00503	65.2	0.99212	0.0015	29.1	0.93916	NA	NA	NA
TiO <sub>2</sub>	0.00351	54.0	0.99865	NA	NA	NA	NA	NA	NA

NA: under the photolysis threshold

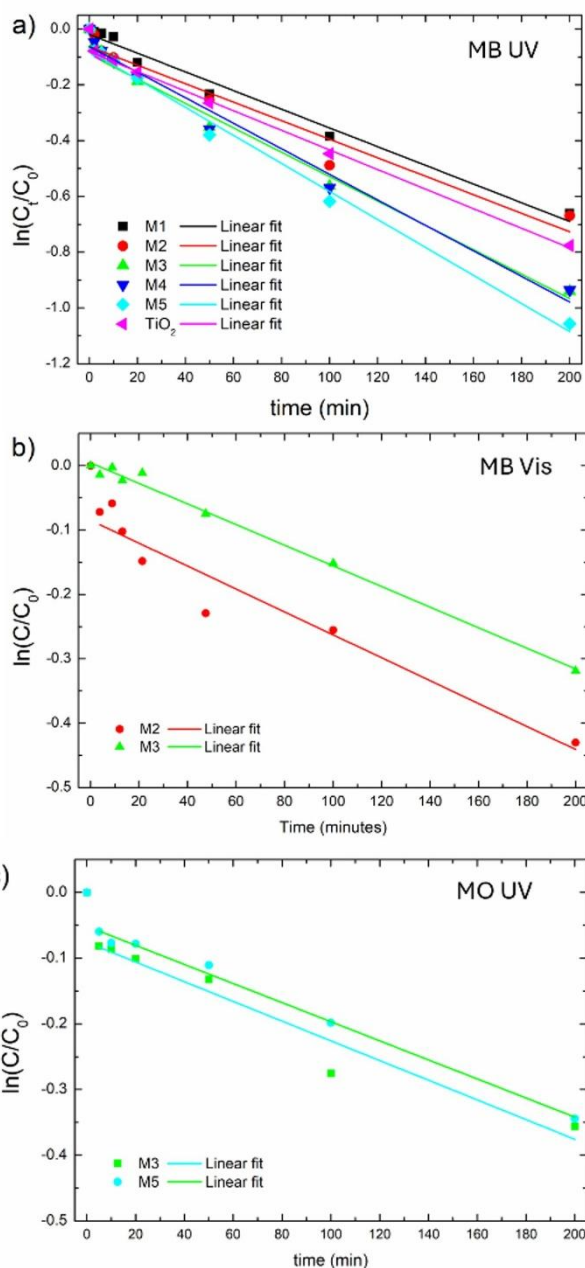


**Figure 8.** Pseudo-first order fitting of the degradation of a) MB with UV light, b) MB with visible light and c) MO with UV light.

MO with UV light (c), fitted with a pseudo-first order kinetic model shown in Equation 3 [12].

$$\ln \frac{C_t}{C_0} = -kt \quad (3)$$

where k refers to the pseudo-first-order rate constant in min<sup>-1</sup>, C<sub>0</sub> is the initial dye and C<sub>t</sub> is the dye concentration at time t from the absorbance data.

Table 1 presents the maximum degradation efficiencies and the pseudo-first order fitting parameters for all the studied materials, dyes and illumination modes.

The fitting quality indicates that the reaction mechanism has additional contributions, therefore, to summarize the ilmenite characteristics with the photodegradation behavior of MB and MO in UV and visible light, Figure 9 shows the proposed electronic band diagrams for the M3-MB and M2-MO systems respectively. The diagrams were built based on the optical band gap, the chemical composition from XRF, the detected crystal phases, and the respective degradation performance of M2 and M3 samples which were the best for the indicated dyes. Supported photocatalysts have strong surface interactions with the adsorbed species such as the dyes [27], but also, free dye interacts with the photoinduced reactive species. The surface interactions are dependent on the presence of active impurities such as V and Mn, which induce surface states and band bending of the main catalyst, TiO<sub>2</sub>, FeTiO<sub>3</sub> or Fe<sub>2</sub>(TiO<sub>3</sub>)<sub>3</sub>.

Figure 9a presents the electronic band diagram for the M3-MB system. This sample, with an optical gap of 2.85 eV, contains crystalline rutile and pseudorutile phases, the maximum V contents of 2 wt% and no Mn. The transient levels of the adsorbed MB (MB<sub>ads</sub>) and the HOMO-LUMO levels of free MB are shown. The impurity levels from V are placed around the valence band minimum and valence band maximum of the main absorber [28]. Upon illumination, photogenerated electrons reach the conduction band from rutile/pseudorutile. The photogenerated holes are injected into the V-occupied states while photogenerated electrons from V-occupied states reach the V-empty levels which are in turn injected into the rutile/pseudorutile conduction band. Electrons promoted to V-empty levels can reduce MB<sub>ads</sub>, while direct transfer from the photogenerated holes can oxidize MB<sub>ads</sub> [27,29]. On the other hand, the MB can be

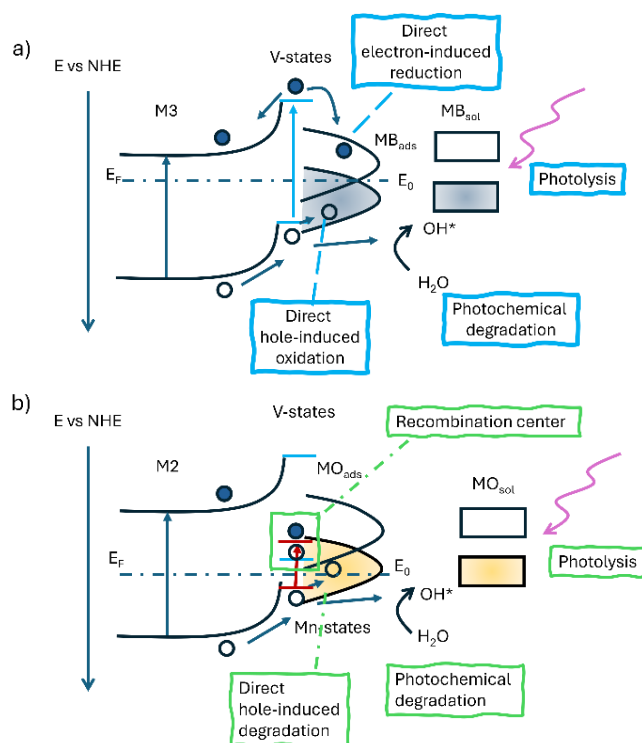


**Figure 9.** Proposed band diagrams of the M3 (a) and M2 (b) ilmenites under UV illumination, showing the extended states assigned to V and, V/Mn respectively, the transient levels of adsorbed MB and MO ( $MB_{ads}$  and  $MO_{ads}$ ), the HOMO-LUMO levels of MB and MO and the photoinduced mechanism occurring at each material under UV illumination. The Fermi level ( $E_F$ ) and relative positions of the V and V/Mn levels were adapted from ref. [28] using the V and Mn concentrations of 2%.

degraded either by photolysis or by the photodegradation process induced by the  $H_2O/OH^*$  reaction at ca. 2.32 V vs NHE. Correspondingly, Figure 9b presents the electronic band diagram of the M2 sample which showed the better photodegradation performance for MO degradation. This sample has a band gap of 2.18 eV and presents mostly ilmenite ( $FeTiO_3$ ) and rutile as crystal phases. On the other hand, M2 has the highest Mn content (ca. 2 wt%) and a V amount of ca. 1.2 wt%. Simultaneous photooxidation and photoreduction of MO was reported by Cañas-Martínez *et al.* for  $(Mn_xFe_{1-x})TiO_2$  ilmenites [29]; however, as shown in Figure 9b, in V-Mn-doped  $TiO_2$  states within the band gap related to Mn(d) and V(d) states create a recombination center above the Fermi level [27], which hinders the direct photoreduction of MO and probably reduces the possibly photooxidation. Therefore, photolysis seems to be the dominant process.

The proposed diagrams explain the low quality of the pseudo-first order fitting and give an insight into the complexity of the photodegradation mechanisms in supported photocatalysts. Additional data from the ilmenites such as z-potential (suspended ilmenites) and point of zero charge (supported ilmenites), as well as the study of photodegradation with different catalyst loads in the formulation and dye concentration in the solutions to separate the surface and free catalyst effects will be subject of future work.

## Conclusions

Five ilmenite minerals were studied for the photocatalytic degradation of methylene blue and methyl orange. UV light degradation in laboratory scale and visible light degradation with pilot-scale reactor (5 L) were tested. The ilmenite samples consisted of rutile ( $TiO_2$ ), pseudorutile ( $Fe_2(TiO_3)_3$ ), and ilmenite ( $FeTiO_3$ ) phases, with Fe/Ti ratios from 1:1 to 10:1; in addition, elements such as V and Mn were present in concentrations ranging 1.6 and 2.3 wt% respectively. The band gap ranged from 2.18 to 2.85 eV, related with Fe/Ti ratio. Samples M3 and M5 with a Fe:Ti ratio of 1:10 and 1:2 respectively, were more efficient than  $TiO_2$  and the other ilmenite samples in the degradation of MB with UV and visible light, while M2, with a ca. 1:1 Fe:Ti ratio, ca. 2 wt% Mn and ca. 1 wt% V, was the best to degrade MO in UV light, surpassing  $TiO_2$ . The photocatalytic degradation curves were fitted to pseudo-first order kinetics, but the deviations from the linear behavior of the  $\log(C_t/C_0)$  vs time plots indicated additional process occurring, specifically direct degradation of adsorbed dyes onto the supported photocatalyst. Electronic band diagrams were proposed to understand the role of V and Mn; V increases the whole degradation by direct MB oxidation and reduction onto the supported photocatalyst by creating states above the maximum of the valence band and the minimum of the conduction band of the absorber, while Mn + V create a recombination center above the Fermi level which hinders direct reduction. A pilot scale reactor was implemented to study MB degradation in a 5 L scale with artificial sunlight. The performance of the supported ilmenites to degrade MB and MO in UV light indicates the feasibility of natural ilmenites for photocatalytic degradation as well as the implementation of a pilot scale reactor, although further studies are considered to optimize the reactor parameters, the photocatalytic formulation and the support features.

## Acknowledgements

This work was financed by SIP-IPN 2025-0311 project. Authors acknowledge the support from Dr. Patricia Quintana for the access to Laboratorio Nacional de Bio y Nanomateriales (LANNBIO) at CINVESTAV-Merida, funded by FOMIX and SECIHTI, and to Daniel Aguilar for XRD measurements.

## References

- [1]. L.I. Diaconu, C.I. Covaliu-Mierlă, O. Păunescu, L.D. Covaliu, H. Iovu, G. Paraschiv, *Biology* **12**, 773 (2023).
- [2]. S.H. Hashemi, M. Kaykhahi, Azo dyes: Sources, occurrence, toxicity, sampling, analysis, and their removal methods. In: *Emerging Freshwater Pollutants*, Eds.: T. Dalu, N.T. Tavengwa, (Elsevier, 2022) p. 267-287.
- [3]. S.N. Tan, M.L. Yuen, R.A. Ramli, *Green Anal. Chem.* **12**, 100230 (2025).
- [4]. Y. Wang, C. Yang, Y. Liu, Y. Fan, F. Dang, Y. Qiu, H. Zhou, W. Wang, Y. Liu, *Water* **13**, 3224 (2021).
- [5]. X. Zhu, J. Wang, D. Yang, J. Liu, L. He, M. Tang, W. Feng, X. Wu, *RSC Adv.* **11**, 27257 (2021).
- [6]. K.M. Mohamed, J.J. Benitto, J.J. Vijaya, M. Bououdina, *Crystals* **13**, 329 (2023).

- [7]. C.B. Anucha, I. Altin, E. Bacaksiz, V.N. Stathopoulos, *Chem. Eng. J. Adv.* **10**, 100262 (2022).
- [8]. K. Nagaraj, S. Radha, C.G. Deepa, K. Raja, V. Umopathy, N. Prakash Badgujar, N.M. Parekh, T. Manimegalai, L. Archana Devi, C. Uthra, *Next Research* **2**, 100180 (2025).
- [9]. H. Moradi, A. Eshaghi, S.R. Hosseini, K. Ghani, *Ultrason. Sonochem.* **32**, 314 (2016).
- [10]. C. Adán, J. Carbajo, A. Bahamonde, A. Martínez-Arias, *Catal. Today* **143**, 247 (2009).
- [11]. R.B. Lee, J.C. Juan, C.W. Lai, K.M. Lee, *Chin. Chem. Lett.* **28**, 1613 (2017).
- [12]. E.Y. Fernando, D. Sarkar, C. Rodwihok, A. Satpathy, J. Zhang, R. Rahmati, R. Datta, C. Christodoulatos, M. Boufadel, S. Larson, Z. Zhang, *Materials* **17**, 3801 (2024).
- [13]. R.A. Putri, S. Tursiloadi, E.F. Nurrahmah, A.R. Liandi, O. Arutanti, *Water Air Soil Pollut.* **234**, 113 (2023).
- [14]. M.E. Besheli, M. Heidari-Golafzani, T. Mohammadi, R. Rahimi, *Results Chem.* **7**, 101297 (2024).
- [15]. H.M. Ali, F.A. Roghabadi, V. Ahmadi, *Solar Energy* **255**, 99 (2023).
- [16]. X. Li, U. Simon, M.F. Bekheet, A. Gurlo, *Energies* **15**, 5607 (2022).
- [17]. C. Guarneros Aguilar, C. Estrada Moreno, M. Pacio Castillo, F. Caballero-Briones, *J. Mater. Sci.* **53**, 1646 (2018).
- [18]. M. Taniguchi, *Absorption coefficient spectrum of Methyl orange. Azo dyes; at PhotochemCAD™ (open in April 2026)*.
- [19]. S. Prah, *Molar Extinction Coefficient for Methylene Blue in Water; at OMLC (open in April 2026)*.
- [20]. O. Monfort, P. Petrisková, *Processes* **9**, 214 (2021).
- [21]. P. Pooseekheaw, W. Thongpan, A. Panthawan, E. Kantarak, W. Sroila, P. Singjai, *Molecules* **25**, 3327 (2020).
- [22]. Q. Luo, X.W. Li, Q.Z. Cai, Q.S. Yan, Z.H. Pan, *Int. J. Miner. Metall. Mater.* **19**, 1045 (2012).
- [23]. P.S. Nair, H. Rahman, J.A. Joseph, A. Norbert, S. Shaji, S. Tripathi, S.N. Jha, R.R. Philip, *Appl. Phys. A* **128**, 1089 (2022).
- [24]. D. Hao, Q. Huang, W. Wei, X. Bai, B.J. Ni, *J. Cleaner Prod.* **314**, 128033 (2021).
- [25]. H. Liang, Z. Wang, L. Liao, L. Chen, Z. Li, J. Feng, *Optik* **136**, 44 (2017).
- [26]. A. Kubiak, M. Jaruga, *Chem. Eng. J.* **510**, 161758 (2025).
- [27]. T. Lana Villarreal, R. Gomez, M. Neumann-Spallart, N. Alonso-Vante, P. Salvador, *J. Phys. Chem. B* **108**, 15172 (2004).
- [28]. R. Rami, N. Rkhioui, R. Ahl Laamara, L.B. Drissi, *Mater. Res. Express* **4**, 126513 (2017).
- [29]. D.M. Cañas-Martínez, G.H. Gauthier, J.A. Pedraza-Avella, *Photochem. Photobiol. Sci.* **18**, 912 (2019).

The results included in this article were presented at the *Renewable Energy: Materials and Devices Simposium, of the XVIII International Conference on Surfaces, Materials, and Vacuum, SMCTSM*, September 22nd to 26th, 2025. Puebla, PUE, Mexico. (see Editorial Note [https://doi.org/10.47566/2026\\_syv39\\_0-260002](https://doi.org/10.47566/2026_syv39_0-260002)).

© 2026 by the authors; licensee SMCTSM, Mexico. This article is an open access article distributed under the terms and conditions of the Creative Commons Attribution license (<http://creativecommons.org/licenses/by/4.0/>).